

Coulomb Blockade and Electron Spin in Quantum Dots

C. M. Marcus¹, J. A. Folk^{1,2}, R. M. Potok¹, A. C. Johnson¹, L. P. Kouwenhoven^{1,3}, R. Berkovits^{4,5,6},
I. L. Kurland⁴, I. L. Aleiner⁷, B. L. Altshuler^{4,5}

¹ *Department of Physics, Harvard University, Cambridge, MA 02138*

² *Department of Physics, Stanford University, Stanford, CA 94305*

³ *Department of Applied Physics and ERATO, Delft University of Technology, Box 5046, GA 2600 Delft, The Netherlands*

⁴ *Physics Department, Princeton University, Princeton, NJ 08544*

⁵ *NEC Research Institute, 4 Independence Way, Princeton, NJ 08540*

⁶ *Minerva Center and Department of Physics, Bar-Ilan University, Ramat-Gan 52900, Israel*

⁷ *Department of Physics, SUNY at Stony Brook, Stony Brook, NY 11794*

We investigate theoretically and experimentally the behavior of Coulomb blockade (CB) peaks in a magnetic field that couples principally to the ground-state spin (rather than the orbital moment) of a quantum dot. In the first part, we discuss numerically observed features in the magnetic field dependence of CB peak spacings that identify changes in spin S of each ground state for successive numbers of electrons on the dot, N . We next evaluate the probability that the ground state of the dot has a particular spin S , as a function of the exchange strength, J , and external magnetic field, B . We then describe experiments on gate-defined GaAs quantum dots in which CB peak motion and spacing are measured as a function of in-plane magnetic field, allowing changes in spin to be measured. Finally, we present recent experiments on phase coherent transport through quantum dots embedded in the two arms of an Aharonov-Bohm ring, in the presence of large in-plane magnetic fields.

I. INTRODUCTION

In the absence of interactions, electrons populate states of a quantum dot in an alternating spin-up – spin-down sequence, such that the total spin of the dot, S , is zero when the number of electrons N on the dot is even, and $S = \frac{1}{2}$ when N is odd; higher spin states do not appear in the absence of large magnetic fields. Interaction can lead to deviations from even-odd filling, as described by the familiar Hund's rules in atomic physics. Hund's rules also apply in symmetric (e.g., circular) quantum dots [14] where interaction can lead to a build-up of ground state spin associated with states that are related by a symmetry of the system. When the quantum dot lacks symmetry or is disordered, degeneracies are not present and the connection between interaction and ground state spin is best described statistically, in terms of mesoscopic fluctuations of the relevant quantities.

By measuring electron transport through a weakly coupled quantum dot at low temperature and bias voltage (compared to the quantum level spacing) one can effectively study differences in ground state (GS) properties of the dot at successive electron number, providing a means of investigating the filling scheme. A standard experimental approach [1] is to measure conduction through the

dot as a function of voltage, V_g , on a nearby capacitively coupled gate. Because the dot GS energy, E_N , at fixed electron number is influenced by V_g , the gate can be used to set the number of electrons on the dot. The fact that a large Coulomb energy is needed to add a single electron to the dot generally suppresses conduction through the dot in the tunneling regime, where whole charges must tunnel for conduction to occur. This effect is known as the Coulomb blockade (CB). At specific values of gate voltage, $V_g^{(N)}$, where $E_{N-1}(V_g) = E_N(V_g)$, conductance increases dramatically, marking this degeneracy condition in an experimental trace. The position, $V_g^{(N)}$, of the N^{th} CB peak is proportional to the electrochemical potential, $\mu_N = E_N(0) - E_{N-1}(0)$. The distance between successive peaks then measures the difference between chemical potentials, $\Delta_2^N = \mu_N - \mu_{N-1}$, and so is a second derivative of GS energy. (We take the constant of proportionality converting gate voltage to dot energy to be unity for the theoretical discussion; experimentally, this constant can be readily measured, for instance, by comparing the influence of bias and gate voltages.)

In the last few years the GS spin of a variety of nanostructures, including metallic dots [2], semiconducting quantum dots [3,4,6], and carbon nanotubes [7,8], have been investigated using CB peak motion in a magnetic field. If the magnetic field coupling to the orbital degrees of freedom can be ignored, the field will manifest itself only through the Zeeman splitting, resulting in a shift of the GS energy by $g\mu_B SB$, where μ_B is the Bohr magneton. For 2D quantum dots, orbital coupling can be strongly suppressed—though not eliminated entirely [9,10]—by orienting the field strictly in the 2D plane. This is the experimental approach that will be described in Section III of this paper. On the other hand, for ultra-small metallic dots and nanotubes, fields in any direction can be considered to act only through the Zeeman effect, since at experimentally reasonable fields the total flux through the structure is small on the scale of the quantum of flux.

For semiconducting quantum dots [3–6] the Zeeman splitting for $S = \frac{1}{2}$ becomes comparable to the mean single electron level spacing

$$\delta_1 = \langle s_i \rangle; \quad s_i = \varepsilon_i - \varepsilon_{i+1}, \quad (1)$$

(here ε_i denotes the orbital energy of the one-electron orbital state i , and $\langle \dots \rangle$ stands for an average over different levels) at $B \sim 1T$ for the GaAs dots is Refs. [4,6] and $B \sim 10T$ for the Si dot in Ref. [3]. At lower fields, the splitting seldom exceeds s_i , and one might expect simple even/odd filling. In this case, CB peak positions would move with Zeeman field, B , (i.e., the magnetic field, ignoring orbital effects) as consecutive pairs, creating a pattern of alternating downward and upward sloped lines with slopes $g\mu_B/2$ and $-g\mu_B/2$ at low field, as seen in Fig. 1a. The peak spacings, Δ_2^N , would have a similar pattern of alternating lines, with slopes of $g\mu_B$ and $-g\mu_B$ as seen in Fig. 1b. Spin-orbit interaction can lead to fluctuations in the g factor, resulting in fluctuations in the slopes of the lines [11,12] but cannot change the pattern of alternating downward and upward lines. Once $g\mu_B B$ exceeds a particular spacing s_i , the peaks would cross as seen in Fig. 1a at higher fields.

Experimentally, simple even/odd filling is observed for the ultrasmall metallic dots [2], while for carbon nanotubes the situation is less clear. One published experiment finds simple even/odd filling [7], and one finds a more complicated scheme [8]. For multielectron semiconducting dots the data are also somewhat confusing, but appear to disagree with the simple even/odd filling scheme at low fields [3–5,13,25]. In symmetric, few-electron vertical dots [14] one may again recover relatively simple behavior for the first few electrons, with a well-understood appearance of Hund’s rules. These conclusions are based on experiments where orbital magnetism dominates spin. However, for few electrons (i.e., $N < \sim 10$) the filling scheme can be readily interpreted, allowing the full spin structure to be mapped out as a function of N and B [14].

Figure 1 shows the theoretical CB peak motion and spacing as a function of Zeeman field for both noninteracting and interacting electrons (as discussed in Section II). The behavior of the interacting case (Fig. 1b) appears more similar to the experimentally observed behavior in semiconducting quantum dots (compare to Fig. 4). In some cases, adjacent peak positions (μ_N) move in the same direction and with the same slope, so that the corresponding spacings (Δ_2^N) are flat as a function of magnetic field. Moreover, not every change in the direction of the motion of a peak can be explained as a crossing of two orbital levels.

The build-up of GS spin in quantum dots has been considered theoretically in a number of different contexts previously [16–23], from providing an explanation [18] for the absence of a bimodal distribution in CB peak spacings [24], to a prediction of kinks in the parametric motion of the peaks due to orbital effects of a perpendicular magnetic field [21], evidence for which is seen in recent experiments [25].

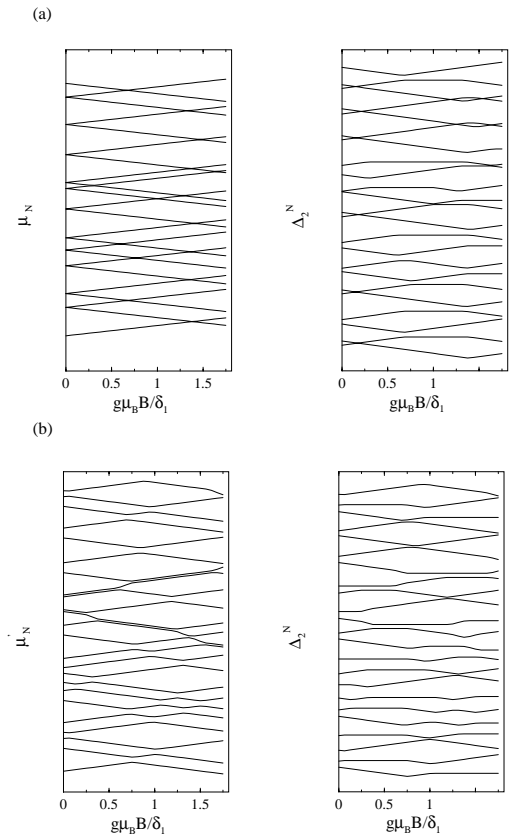


FIG. 1. Typical conductance dependence on the gate voltage and magnetic field, B , with and without exchange interaction: (a) $J = 0$, (b) $J = 0.1\delta_1$. μ'_N is determined as $\mu'_N = \mu_N - e^2/C$ and taken in arbitrary units. Δ_2^N for each N is shifted arbitrarily by $N \times \text{constant}$ to avoid overlapping.

II. THEORY

The single electron spectrum ε_i in disordered or irregularly shaped quantum dots is characterized by the mean level spacing δ_1 and the Thouless energy $E_T \approx \hbar/t_{erg}$, where t_{erg} is the time it takes for a classical electron to cover the energy shell in the single-particle phase space. For either diffusive or ballistic-chaotic systems, t_{erg} is roughly given by the crossing time, L^2/D and L/v_F respectively, where v_F is the Fermi velocity, L is the system size, and D is the diffusion coefficient. The dimensionless conductance, $g_T = E_T/\delta_1$, in the metallic regime is large, $g_T \gg 1$. In this regime the statistics of the single electron spectrum on scales smaller than E_T are well described by random matrix theory (RMT) [26], which gives a quantitative description of the phenomenon of level repulsion. For an ensemble of $M \times M$ matrices ($M \rightarrow \infty$) with random and independent elements, the probability density of a realization of the spectrum ε_i is given by [26]:

$$P(\varepsilon_i) \propto \exp \left[\frac{\beta}{2} \sum_{i \neq j} \ln \left(\frac{|\varepsilon_i - \varepsilon_j|}{\delta_1} \right) \right], \quad (2)$$

where β is equal to 1, 2 or 4 for the orthogonal, unitary and symplectic ensembles respectively. The orthogonal (unitary) RM ensemble corresponds to preserved (violated) time reversal symmetry and negligible spin-orbit. The role of spin-orbit interaction in quantum dots has recently been considered experimentally and theoretically [5,15,27,10], and it has been shown [27] that the combination of spin-orbit interaction and Zeeman field produces new universality classes, generalizing the Dyson ensembles ($\beta = 1, 2, 4$).

Electron-electron interaction can be accounted for, in the simplest case of short-range interactions, by an interaction term in the Hamiltonian,

$$H_{int}(\vec{r}) = \lambda \delta_1 V \delta(\vec{r}), \quad (3)$$

where $V \propto L^d$ is the volume of the dot (in d dimensions) and λ is a dimensionless coupling constant characterizing the strength of the interaction. Matrix elements of this interaction, in the basis of eigenstates $\varphi_i(\vec{r})$ of the noninteracting Hamiltonian, are given by

$$M_{kl}^{ij} = \lambda \delta_1 V \int d\vec{r} \varphi_i^*(\vec{r}) \varphi_j^*(\vec{r}) \varphi_k(\vec{r}) \varphi_l(\vec{r}). \quad (4)$$

It is important to note that the statistical properties of the interaction matrix elements M_{kl}^{ij} are completely determined by the statistical properties of the single electron eigenstates $\varphi_i(\vec{r})$ and cannot be chosen in an arbitrary fashion as in the random interaction model [22]. In fact, in the limit $g_T \rightarrow \infty$ the diagonal matrix elements (i, j, k, l pairwise equal) are self-averaged by the space integration, Eq. (4), and thus show no level-to-level or sample-to-sample fluctuations [16]. In the same limit the off-diagonal matrix elements Eq. (3) turn out to be negligible.

Using the statistical properties of the interaction matrix elements it turns out that a large class of disordered metallic dots can, under very general conditions, be described by a remarkably simple Hamiltonian with only three system-dependent coupling constants, which do not fluctuate. In the limit of large g_T , the interaction part of the Hamiltonian corresponds to

$$H_{int} = E_c \hat{N}^2 - J(\vec{S})^2 + \lambda_{BCS} \hat{T}^\dagger \hat{T}, \quad (5)$$

(terms linear in \hat{N} are allowed, but they can be included into the one-particle part of the Hamiltonian) where \hat{N} is the number operator, \vec{S} is the spin operator and $\hat{T} = \sum_i c_{i\uparrow} c_{i\downarrow}$ ($c_{i\uparrow}$ annihilates an electron in the i^{th} single electron orbital with spin \uparrow). In the simple model with short-range interaction and preserved time reversal ($\beta = 1$) the coupling constants have the following form:

$$E_c = \frac{1}{2} \lambda \delta_1; \quad J = 2 \lambda \delta_1; \quad \lambda_{BCS} = \lambda \delta_1. \quad (6)$$

If time invariance is broken ($\beta = 2$), $\lambda_{BCS} = 0$ since the operator \hat{T} is incompatible with the symmetry. Note that the interaction Hamiltonian Eq. (3) represents a particular model, and the expressions for the coupling constants Eq. (6) are valid only for this model. At the same time, the effective interaction Hamiltonian, Eq. (5), is more robust and depends only on the symmetries of the problem (for instance, on the absence of the spin-orbit scattering) and on the condition $g_T \gg 1$.

The first two terms in Eq. (5) represent the dependence of the energy of the dot on the total number of the electrons and on the total spin respectively. They commute with each other and with the single-particle part of the Hamiltonian. Therefore, all states of the dot can be classified by N and S . The term proportional to λ_{BCS} appears only in the orthogonal case ($\beta = 1$) and provided that $\lambda_{BCS} < 0$ this term leads to a superconducting instability. Superconducting correlations are suppressed by the magnetic field, and thus do not exist for $\beta = 2$.

Thus, the general form of the Hamiltonian describing electrons in a disordered or chaotic (non-superconducting) dot with $g_T \gg 1$ is given by

$$H = \sum_i \varepsilon_i n_i + E_c N^2 - JS(S+1) + g\mu_B SB. \quad (7)$$

Note that the only random component of the problem is the single-particle spectrum ε_i , while the exchange J and charging energy E_c do not fluctuate.

The conductance is calculated using the many-particle energies E_N and wave functions obtained numerically for random matrix realizations. An example of the peak positions and peak spacing evolution as functions of the magnetic field for a particular GOE realization is shown in Fig. 1 for (a) $J = 0$ and (b) $J = 0.1\delta_1$. For both cases we present $\mu'_N = \mu_N - E_c$. The noninteracting case, Fig. 1a, shows all the previously described features of the simple even/odd filling behavior. When a weak exchange interaction is included the behavior changes qualitatively. In particular, peak positions are not always paired. This occurs when two consecutive orbitals are first filled with down spin electrons and only later they acquire up electrons. Note that the enhancement of the spin of the dot by S is indicated by a sequence of $2S$ peaks moving with the same slope. If the peak spacing Δ_2^N is plotted, two sets of $2S - 1$ flat curves sandwiching a sloped one will appear.

Equation (7) can be used to estimate the probability distribution of GS spins. For weak exchange, $J \ll \delta_1$, the probability that the GS has spin S is simply the probability of finding $2S$ orbital levels sufficiently close that the reduction in energy due to exchange exceeds the excess kinetic energy needed fill the higher orbital levels,

$$\varepsilon_{i+2S} - \varepsilon_i < JS(S+1) + g\mu_B BS. \quad (8)$$

Using the random matrix distributions of level spacings, Eq. (2), one finds the probability of obtaining a ground state spin S can be written a function of the linear combination

$$X = \frac{J}{\delta_1} + \frac{g\mu_B B}{[S + \frac{3}{2}]\delta_1}, \quad (9)$$

giving a probability distribution for spin S ,

$$P_{J,B}(S) = C_S^\beta X^{(\beta S+1)(2S-1)}(1 - K_S^\beta X^2), \quad (10)$$

where coefficients C_S^β and K_S^β depend on both β and S . Their values for $S = 1, 3/2$ are presented in table I.

	$\beta = 1$		$\beta = 2$	
	$S = 1$	$S = 3/2$	$S = 1$	$S = 3/2$
C	$\pi^2/3$	$9\pi^4/50$	$8\pi^2/9$	$81\pi^6/400$
K	$\pi^2/5$	$18\pi^2/49$	$8\pi^2/25$	$792\pi^2/1225$

TABLE I. The factors C_S^β and K_S^β appearing in Eq. (10).

The important conclusion from RMT is that the combined influence of exchange and Zeeman field on the GS spin of a quantum dot can be expressed as a single scaling parameter that is a linear combination of J and B . Numerical simulations confirm this scaling and show, in fact, that it continues to hold for larger values of X than expected from the perturbative analysis leading to Eq. (10).

Whether these results continue to apply when $g_T \sim O(1)$ can be addressed numerically within a Hubbard model approach, described by the Hubbard Hamiltonian

$$H = \sum_{i,\sigma} \epsilon_i a_{i,\sigma}^\dagger a_{i,\sigma} - t \sum_{\langle i,j \rangle, \sigma} (a_{i,\sigma}^\dagger a_{j,\sigma} + h.c.) + U \sum_i a_{i,\uparrow}^\dagger a_{i,\uparrow} a_{i,\downarrow}^\dagger a_{i,\downarrow} + g\mu_B S B, \quad (11)$$

where $\langle i, j \rangle$ denotes nearest neighbor lattice site, $a_{i,\sigma}^\dagger$ is an creation operator of an electron at site i with spin σ , ϵ_i is the site energy, chosen randomly between $-W/2$ and $W/2$ with uniform probability, and U is the interaction constant. Note that this problem becomes quite difficult numerically even for relatively small systems. For instance, a 4×4 lattice with 6 electrons for the $S = 0$ sector has a Hilbert space of 313,600 states. Using the Lanczos method we obtain the many-particle eigenvalues $E_N(S)$ for different values of interaction U , as shown in Fig. 2. For these data, disorder was fixed at $W = 8t$, which corresponds to the metallic regime although the value of the dimensionless conductance is quite low, $g_T \sim O(1)$.

We calculated the probability for the appearance of a specific value of GS spin S for different values of U and magnetic field B . In order to use the scaling parameter X we need to deduce the appropriate value of J for each

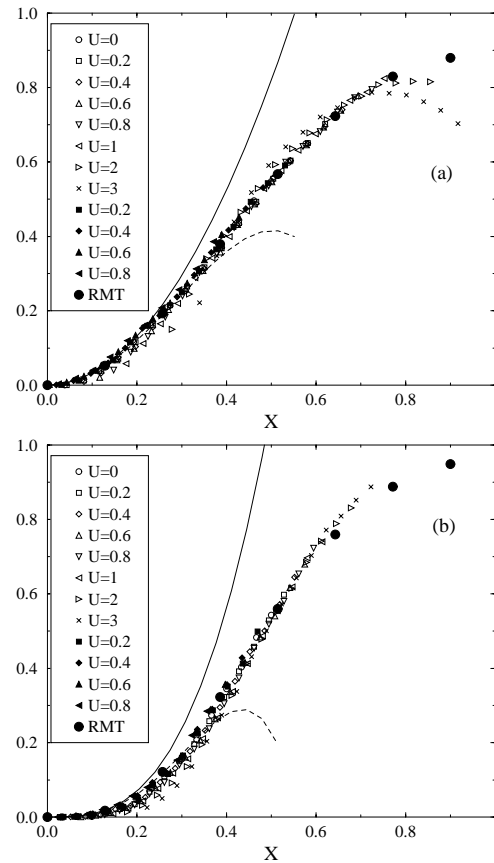


FIG. 2. Probabilities of $S = 1$ for $J = 0.1\delta_1$ as functions of the magnetic field B for (a) the GOE and (b) GUE cases. The small symbols represent numerical results for the Hubbard model, the large filled symbols represent numerical results for the RMT model, while the curves (solid - first order, dashed - second order) represent Eq. (10).

value of U . This has been done by fitting the dependence of the average lowest energy in a given spin sector $\langle E(S) \rangle$ to

$$\langle E(S) \rangle = \delta_1 S^2 - JS(S+1). \quad (12)$$

The distribution $P_{J(U),B}(S)$ based on numerical results for 1000 different realizations of the Hubbard model, for different values of U and B for $\beta = 1$ and $\beta = 2$ is presented in Fig. 2 [28]. Although some deviations from Eq. 10 are seen, especially for the higher values of U , the overall form of the scaling function holds remarkably well.

III. EXPERIMENT: GROUND STATE MEASUREMENT

In this section we describe experimental measurements of GS spin for a single gate-defined GaAs quantum dot containing roughly 400 electrons. The dot is coupled to

electron reservoirs via tunnelling leads (i.e., $g < 2e^2/h$ for both leads) so transport is dominated by CB effects. Measurements were carried out at sufficiently low temperature and bias that the differences in GS energies between dots with $N - 1$ and N electrons should be extractable from CB peak positions, $V_g^{(N)}$.

The dot is formed at the interface of a GaAs/AlGaAs heterostructure (90 nm below the wafer surface) by electrostatic depletion using surface gates. The two-dimensional electron gas (2DEG) has density $\sim 2.0 \times 10^{11} \text{ cm}^{-2}$ and bulk mobility $\sim 1.4 \times 10^5 \text{ cm}^2/\text{Vs}$, yielding a transport mean free path $\sim 1.5 \mu\text{m}$. The small dot area, $A \sim 0.25 \mu\text{m}^2$, makes transport predominantly ballistic within the device. Characteristic energy scales for the measured device include the mean level spacing, $\Delta = 2\pi\hbar^2/m^*A \sim 30 \mu\text{eV}$, the charging energy, $E_C \sim 400 \mu\text{eV}$, and the Thouless energy $E_{th} = \hbar v_F A^{-\frac{1}{2}} \sim 340 \mu\text{eV}$. Measurements were carried out in a dilution refrigerator using standard ac lock-in techniques with a source-drain bias voltage of $2 \mu\text{eV}$. A base electron temperature of $T_e \sim 50 \text{ mK}$ was determined from CB peak widths.

To allow the magnetic field to couple predominantly to spin, the sample was oriented with the plane of the electron gas along the axis of the primary solenoid, aligned manually to within 0.5 degrees. In addition, a pair of coils attached to the vacuum can of the fridge, oriented perpendicular to the plane of the sample, was used to null out any perpendicular field from misalignment as well as to explicitly break time-reversal symmetry [5]. The estimated uncertainty in B_\perp is less than $\phi_o/4$ through the dot at $B_\parallel = 5 \text{ T}$. Despite this precise field trimming capability, similar measurements [5] in larger dots indicate orbital coupling even from a perfectly aligned field (evident, for instance, in the complete disappearance of weak localization $B_\perp = 0$ at higher B_\parallel). The estimated flux coupling due to an in-plane field appears consistent with recent theoretical estimates [9]; experiments to separate the influences of the spin-orbit coupling and in-plane flux coupling are now underway [10].

Conductance measurements across ten consecutive Coulomb blockade peaks, measured as a function of V_g and B_\parallel (i.e., *strictly* B_\parallel , properly trimmed), are shown in grayscale in Fig. 3a. More positive gate voltage corresponds to higher energy, and can be calibrated from the CB “diamonds” using high source-drain bias measurements [1]. All data are taken with $B_\perp = 20 \text{ mT}$ in order to ensure that time-reversal symmetry is broken.

In addition to the linear motion of individual peaks, there is an overall parabolic shift of all peaks (see Fig. 3b), presumably due to the diamagnetic effect of the in-plane field on the effective well confinement potential. A paramagnetic shift is also visible at very low field, ($B_\parallel < 0.2 \text{ T}$), and is not understood at present. In the analysis presented, the common curve (in Fig. 3b) has been subtracted from each peak position.

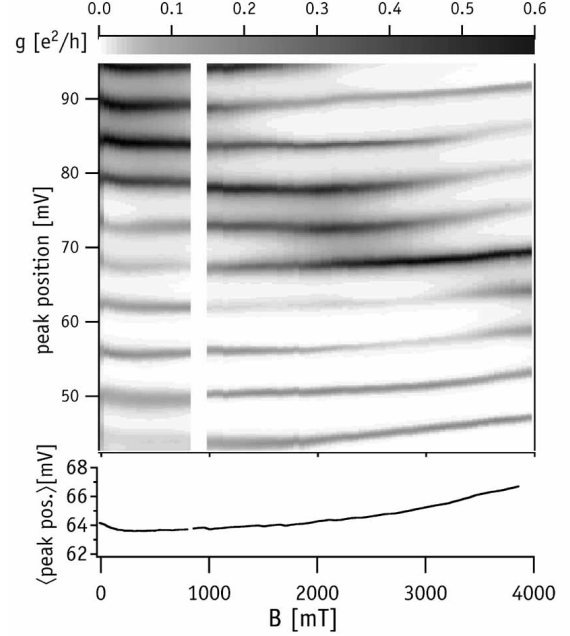


FIG. 3. a) Nine consecutive Coulomb blockade peaks measured as a function of gate voltage V_g and parallel field B . Conductance is shown in grayscale, with black indicating high conductance and white low conductance. The field shown on the bottom axis is the field strictly parallel to the heterointerface; perpendicular field is held constant at 20 mT as discussed in the text. Note that conductance in the valleys is low but not zero, due to strong tunnelling in the leads. b) Average peak position of the peaks in a), showing a diamagnetic shift to higher energies common to all peaks. This average is subtracted from all peak positions before further analysis.

Positions and spacings from the peaks in Fig. 3 are shown in Fig. 4. The slopes of peak position as a function of B_\parallel are consistent with a Zeeman energy term $E_S = \pm \frac{1}{2} g \mu_B B_\parallel$, using the g -factor for bulk GaAs, $|g| = 0.44$. As discussed in the Introduction, alternating slopes (as a function of B_\parallel) of peak position would indicate GS spins alternating between $S = 0$ and $S = \frac{1}{2}$. The experimental data, on the other hand, shows several pairs of consecutive peaks moving with the same slope, implying the presence of higher-spin ground states. Proposed values for the eight consecutive GS spin states shown here are included in Fig. 4a. We emphasize, however, that these are only suggested values for the spin; it is not possible to unambiguously determine the GS spin from measurements of peak position, which reflect *changes* in spin from the $N-1$ to N ground states.

In the proposed spin labelling scheme, three out of the five even- N states have $S = 1$, i.e., $P(S = 1) \sim 0.6$. This fraction of $S = 1$ relative to the number of $S = 0$ states is greater than expected given reasonable estimates of J for

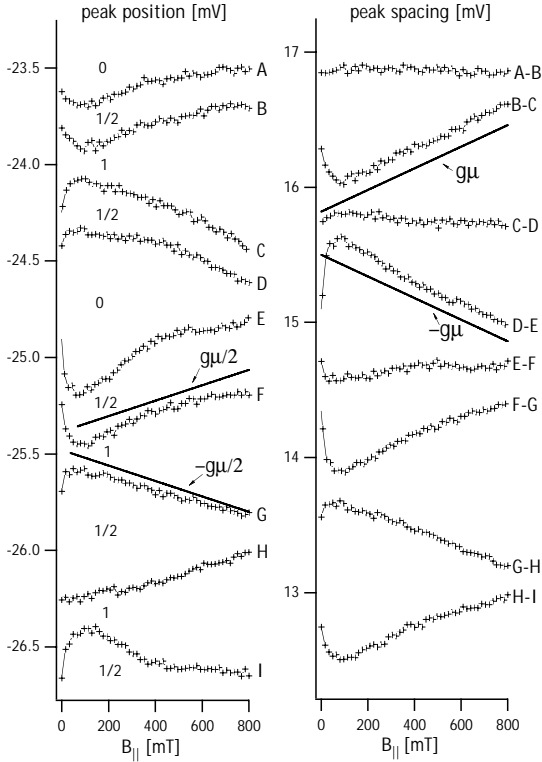


FIG. 4. a) Peak positions (with average motion subtracted) as a function of parallel field for the nine peaks shown in Fig. 3a. Straight lines indicate expected peak motion for $\Delta S = \frac{1}{2}$ transitions using the g factor for bulk $GaAs$, $|g| = 0.44$. Positive slopes indicate transitions to lower spin states; negative slopes indicate transitions to higher spin states. Numbers indicate a possible ground-state spin structure for ten consecutive ground states. Peak position data are offset for clarity. b) Peak spacings for the position data shown in a), offset for clarity. Solid lines indicate expected motion of peak spacing for spin- $\frac{1}{2}$ transitions, using $|g| = 0.44$.

$GaAs$ dots. Of course, with only five spin states considered, statistics are rather poor. Experiments currently in progress aim to greatly augment these statistics.

Figure 5 shows that the peak spacings (the same data as in Fig. 4) clearly separate into three branches, a top branch with slope $\sim g\mu_B$ (corresponding to a GS spin decrement followed by an increment) a bottom branch with slope $\sim -g\mu_B$ (corresponding to a GS spin increment followed by a decrement) and a middle branch with slope near zero (corresponding to two consecutive increments or decrements). *The existence of this middle branch is the signature of higher GS spin states.* The good agreement between the slopes of the upper and lower branches and the expected slopes of $g\mu_B$, as well as the absence of a range of intermediate slopes suggest that the peak spacing reflects spin rather than orbital motion of levels. At higher fields, the directions of peak motion change, often abruptly and from one straight segment to another, as seen in Fig. 6. This behavior is qualitatively

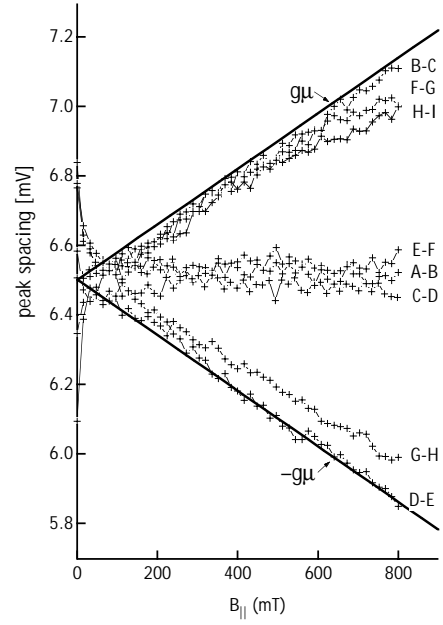


FIG. 5. Peak spacings from Fig. 4b, offset to align spacings at $B_{||} = 0$. Slopes cluster in three branches, interpreted as a change from decreasing to increasing spin transitions (positive slope), two consecutive spin transitions in the same direction (zero slope), and a change from increasing to decreasing spin transitions (negative slope). Solid lines indicate expected motion of peak spacing for spin- $\frac{1}{2}$ transitions, using $|g| = 0.44$, with no adjustable parameters.

similar to the numerical data in Fig. 1b. The rounding of straight segments where the slope changes presumably results from spin-orbit interaction which mixes spins, and may provide a direct measure of spin-orbit interactions in dots. It is interesting to note that the peaks analyzed in Figs. 4 through 6 were measured in a regime of high tunneling conduction in the leads. This can be seen by noting the grayscale of Fig. 3. When the dot is more pinched off from the reservoirs, so that the CB peaks have a height of $0.1 e^2/h$ or less, peak motion is more difficult to interpret, and does not seem to follow the clear patterns illustrated. This is not understood at present, and will be investigated further.

IV. EXPERIMENT: COHERENT TRANSPORT OF SPIN AND CHARGE

In a large in-plane magnetic field ($g\mu_B B_{||} \gg kT$) and low temperatures ($\Delta \gg kT$) transport on a CB peak marks a transition between ground states with well defined spin projections, m_S , along the direction of the applied field. Consider, for instance, the CB peak between $N - 1$ and N electrons on the dot with $N - 1$ even and GS spins $S^{(N-1)} = 0$ and $S^{(N)} = \frac{1}{2}$: Transport on the peak involves a spin up electron passing through the dot (for the sake of the argument, we do not account for the

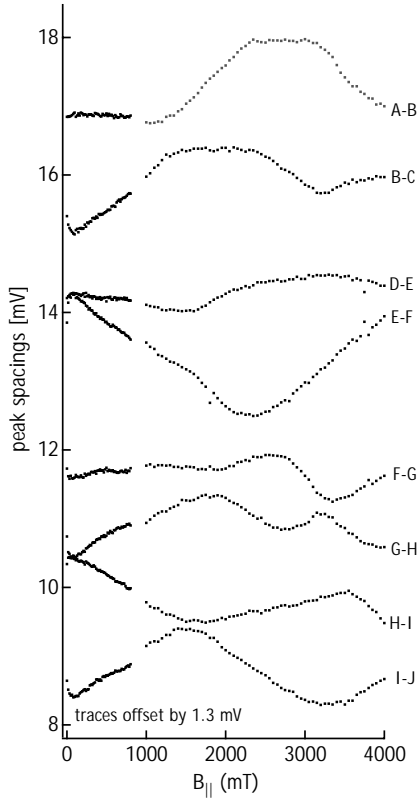


FIG. 6. Peak spacings from Fig. 6b, shown over an extended range of parallel field, up to $B_{\parallel} = 4T$. Slopes tend to change abruptly between linear segments, with rounding between the segments possibly providing a measure of spin-orbit or other spin-mixing interaction.

negative g factor), involving the transition from $m_S = 0$ to $m_S = \frac{1}{2}$ when the electron enters, and from $m_S = \frac{1}{2}$ to $m_S = 0$ when the electron leaves. One may examine the coherence of this spin-selective transport process by embedding the quantum dot in the arm of an Aharonov-Bohm (AB) ring [29], as shown in Fig. 7.

In the experiment reported here, two gate-defined quantum dots are used, one in each arm of an AB ring (Fig. 7). This configuration allows a comparison of two situations of interest: (i) both dots have N even or N odd, which should allow an electron with a given m_S to pass through either arm and (ii) one dot has N even and one dot has N odd, which should allow a particular electron of a given m_S to only pass through one of the two arms. The latter situation is analogous to a two-slit interference experiment in classical optics, in which two polarizers oriented at 90 degrees are each placed in front of one of the slits. The expectation is that the situation (ii) will show a suppressed interference signal relative to situation (i). A detailed theoretical analysis of related configurations involving one or two dots embedded in AB rings, and the interplay between spin and coherence in such systems, is discussed in Ref. [30]. This paper

also provides a useful guide to the rapidly growing literature surrounding dot-in-ring configurations. The present ‘spin-filters-in-rings’ set-up, i.e., dots in a ring in a large in-plane field, has not been considered experimentally or theoretically to our knowledge.

A micrograph of an AB device identical to the one measured is shown in Fig. 7b. The ring encloses an area of $\sim 3.5\mu\text{m}^2$, setting a perpendicular field of $\sim 1.2\text{mT}$ to thread one flux quantum through the ring. The dots have an area of $\sim 0.04\mu\text{m}^2$, giving a quantum level spacing of $\sim 1\text{K}$. Measurements were carried out in a dilution refrigerator at an electron temperature of $\sim 80\text{mK}$.

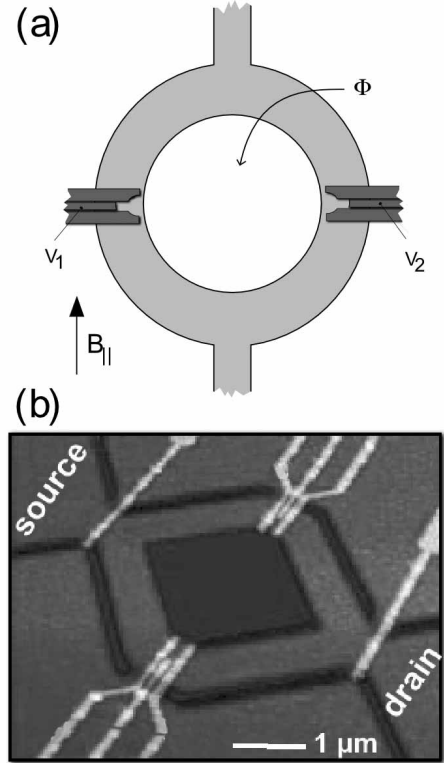


FIG. 7. (a) Schematic set-up of quantum dot interferometer, comprising two quantum dots in the arms of a two-lead Aharonov-Bohm ring. An in-plane magnetic field B_{\parallel} is used to polarize electrons while a small, independent perpendicular field is used to modulate the relative phase of electrons passing through the two arms of the interferometer. (b) An electron micrograph of a Delft interferometer, identical in size and design to the one in that was used in the measurement described in Section IV.

Differential conductance measured at finite source-drain bias is used to characterize spin transition between ground states of the $N - 1$ and N electron dots ground states by looking at the evolution of excited-state features of the N^{th} CB peak as a function of in-plane field. Following the method used to deduce ground state spin transitions in nanotubes [7] (see also a related approach

used in ultrasmall metal dots [2]), we find a Zeeman splitting either on the left side of the CB region (Fig. 8a), indicating a transition from S to $S + \frac{1}{2}$, or a Zeeman split peak on the right side (Fig. 8b), indicating a transition from $S + \frac{1}{2}$ to S . A clear discussion of how spin transitions lead to these associated patterns of Zeeman splitting in nonlinear transport can be found in Ref. [7]. The fact that these patterns are observed in the present measurement means, for instance, that the temperature is sufficiently low that the Zeeman split levels can be resolved.

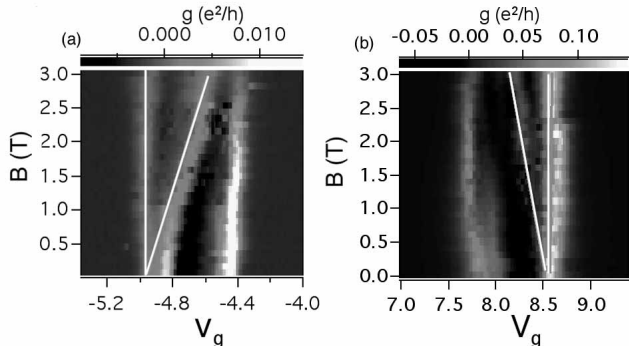


FIG. 8. Grayscale plot of differential conductance across a broadened CB peak at finite source-drain voltage, ($V_{sd} = 0.12$ mV in (a) and 0.15 mV in (b)), as a function of in-plane magnetic field. Internal structure shows Zeeman splitting either on the left (a) or the right (b) edge of the peak, indicates a spin-increasing or spin-decreasing transition between $N - 1$ and N [7]. The white lines are guides to the eye. (a) and (b) are for consecutive peaks in dot 2, with dot one fully pinched off, blocking arm 1 of the interferometer.

The initial experiments presented here have focused on two questions in particular: first, is transport in this system with a large in-plane field—when the dots are expected to act as spin filters—phase coherent? And second, is quantum interference affected by changing N in one of the dots, which we expect to reverse the orientation of the filters in one of the arms, while N and hence the filter orientation in the other arm is held fixed.

Experimental results are shown in Fig. 9. On the left is a grayscale plot of conductance of the full device as a function of gate voltages, V_1 and V_2 , of the dots in the two arms, with an in-plane field $B_{\parallel} = 6$ T. Clearly visible in this plot is one vertical stripe, marking a CB peak in dot 2, and several horizontal stripes, marking CB peaks in dot 1. The intersections of the stripes mark where both dots are on CB peaks. The intersection points of the two stripes are the points where we would expect independent spin filtering in each of the arms to occur. On the right of Fig. 9 are sweeps of perpendicular field (with $B_{\parallel} = 6$ T held constant) taken at each of the points of intersection of the CB stripes. AB oscillations are clearly visible in each of the traces, on a field scale consistent with one quantum of flux through the area enclosed by the ring.

This answers the first question, posed above: Transport through the ring and the two quantum dots in a large in-plane field is at least partially coherent. The amplitude of the AB oscillations was $\sim 10\%$ of the total conductance, and did not appear to depend on the value of in-plane field.

We did not observe a systematic dependence of AB amplitude upon changing N in dot 1, however. We do not think that this absence is explained by a lack of even/odd filling; over the several peaks examined, we would expect at least one upward and one downward spin transition in the set of five intersections. We do not know at this point why a clear signature of spin filtering in the arms was not observed. It is worth noting however, that few CB peaks could be resolved in these devices. Estimates of spin-orbit scattering rates in the arms of the ring do not make this a likely reason for the absence of a filtering effect, either. Fabrication is currently underway to build devices that would allow greater control of dot coupling parameters to continue to explore this interesting system.

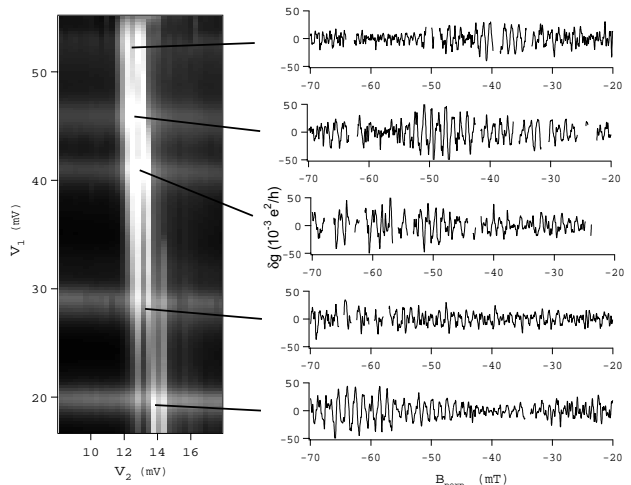


FIG. 9. Left: Grayscale plot of two-lead conductance of AB ring as a function of center gate voltages on the dots in the two arms, in the CB regime. Vertical and horizontal stripes mark CB peaks in each of the arms. Right: AB conductance oscillations measured for a fixed CB peak for dot 2 and consecutive peaks in dot 1. No systematic dependence on electron number is observed in this small data set.

V. CONCLUSIONS

In conclusion, we have investigated the interplay of interactions, spin, and (preliminarily) phase coherence in quantum dots the Coulomb blockade regime. In section II, we presented calculations of the probability that different values of ground state spin appear as a function of exchange interaction and magnetic field coupling

to the spin. We find that the probability density is described by a one-parameter scaling law over a surprisingly wide range of magnetic fields and exchange interaction strengths.

We also described experiments investigating ground state spins of quantum dots using CB peak motion in a single gate-confined GaAs quantum dot. The experimental signature of nonminimal ground state spin is CB peak spacings with zero slope as a function of in-plane magnetic field. Such signatures are seen in several cases in the data. Further experiments are needed to obtain sufficient statistics to quantitatively test the predictions of theory.

Finally, we described preliminary experiments on phase coherent transport through quantum dots embedded in the two arms of an Aharonov-Bohm ring, in the presence of large in-plane fields. In this situation, the dots are expected to function as spin filters. Quantum interference is observed, in the form of periodic AB conductance oscillations as a function of perpendicular magnetic field. No systematic dependence on the number of electrons in dots is found, for reasons not presently understood. Further fabrication and experiments in this direction are underway.

VI. ACKNOWLEDGEMENTS

Support from ARO-MURI DAAG55-98-1-0270 and the DARPA QuIST Program is gratefully acknowledged. JAF acknowledges support as a DoD Fellow; RMP acknowledges support as an ARO graduate fellow; ACJ acknowledges support as an NSF fellow. We thank P. W. Brouwer, B. I. Halperin and L. P. Rokhinson for many useful discussions, and S. M. Cronenwett for assistance with experiments and analysis. The device discussed in Section II was fabricated by S. R. Patel (Stanford) on material grown by C. I. Duruöz in the lab of J. S. Harris, Jr. (Stanford). The device discussed in Section III was fabricated by W.G. van der Wiel (T.U.Delft) and T. Fujisawa (N.T.T.).

- [6] J. A. Folk *et al.*, Physica Scripta **T90**, 26 (2001), (also, cond-mat/0010441).
- [7] D. H. Cobden *et al.*, Phys. Rev. Lett. **81**, 681 (1998).
- [8] S. J. Tans *et al.*, Nature **393**, 49 (1998).
- [9] V. I. Falko and T. Jungwirth, cond-mat/0106019 (2001).
- [10] D. M. Zumbühl, J. B. Miller, C. M. Marcus, J. S. Harris, Jr., in preparation (2001).
- [11] K. A. Matveev, L. I. Glazman and A. I. Larkin, Phys. Rev. Lett. **85**, 2789 (2000).
- [12] P. W. Brouwer, X. Waintal and B. I. Halperin, Phys. Rev. Lett. **85**, 369 (2000).
- [13] D. R. Stewart *et al.*, Science **278**, 1784 (1998).
- [14] S. Tarucha *et al.*, Phys. Rev. Lett. **77**, 3613 (1996).
- [15] B. I. Halperin, *et. al.*, Phys. Rev. Lett. **86**, 2106 (2001).
- [16] I. L. Kurland, I. L. Aleiner and B. L. Altshuler, Phys. Rev. B **62**, 14886 (2000).
- [17] A. V. Andreev and A. Kamenev, Phys. Rev. Lett. **81**, 3199 (1998).
- [18] R. Berkovits, Phys. Rev. Lett. **81**, 2128 (1998).
- [19] P. W. Brouwer, Y. Oreg and B.I. Halperin, Phys. Rev. B **60**, R13977 (1999).
- [20] E. Eisenberg and R. Berkovits, Phys. Rev. B **60**, 15261 (1999).
- [21] H.U. Baranger, D. Ullmo and L.I. Glazman, Phys. Rev. B **61**, R2425 (2000).
- [22] P. Jacquod and A. D. Stone, Phys. Rev. Lett. **84**, 3938 (2000).
- [23] Y. Oreg, P. W. Brouwer, X. Waintal, B. I. Halperin, cond-mat/0109541 (2001).
- [24] U. Sivan, *et al.*, Phys. Rev. Lett. **77**, 1123 (1996); F. Simmel, *et al.*, Europhys. Lett. **38**, 123 (1997); S.R. Patel, *et al.*, Phys. Rev. Lett. **80**, 4522 (1998); F. Simmel, *et al.*, Phys. Rev. B **59**, R10441 (2000).
- [25] S. Lüscher, *et al.* Phys. Rev. Lett. **86**, 2118 (2001).
- [26] M. L. Mehta *Random Matrices*, (Academic Press, NY, 1991).
- [27] I. L. Aleiner and V. I. Falko, cond-mat/0107385 (2001).
- [28] I. L. Kurland, R. Berkovits and B. L. Altshuler, Phys. Rev. Lett. **86**, 3380 (2001).
- [29] A. Yacoby, M. Heiblum, D. Mahalu, and H. Shtrikman, Phys. Rev. Lett. **74**, 4047 (1995).
- [30] J. König and Y. Gefen, cond-mat/0107450 (2001).

-
- [1] M. A. Kastner, Rev. Mod. Phys. **64**, 849 (1992); R. C. Ashoori, Nature **379**, 413 (1996); Kouwenhoven *et al.*, in *Mesoscopic Electron Transport*, Ed. by L. L. Sohn, L. P. Kouwenhoven, and G. Schön (Kluwer, Dordrecht, 1997).
 - [2] D. C. Ralph, C. T. Black and M. Tinkham, Phys. Rev. Lett. **74**, 3241 (1995).
 - [3] L. P. Rokhinson *et al.*, Phys. Rev. B **63** 5321 (2001).
 - [4] D. S. Duncan *et al.*, Appl. Phys. Lett. **77**, 2183 (2000).
 - [5] J. A. Folk *et al.*, Phys. Rev. Lett. , in press, (2001), (also, cond-mat/0005066).